CrossMark

ORIGINAL PAPER

Effects of crosslinked elastomer particles on heterogeneous nucleation of isotactic PP in dynamically vulcanized EPDM/PP and EOC/PP blends

Nattapon Uthaipan[1] · Methakarn Jarnthong[2] · Zheng Peng[2] · Banja Junhasavasdikul[3] ·
Charoen Nakason[4] · Anoma Thitithammawong[1] (ORCID)

Abstract The isothermal and non-isothermal crystallizations of PP in neat form and in the TPVs EPDM/PP and EOC/PP were investigated using differential scanning calorimetry (DSC). The crystallization of PP was systematically studied by fitting mathematical models, and was later confirmed by X-ray diffraction (XRD) and by scanning electron microscopy (SEM). The experiments revealed that crosslinked elastomer particles first accelerated the primary nucleation of the PP matrix, acting effectively as a nucleating agent that reduces the induction time while increasing the nucleation efficiency. In the secondary nucleation regime (growth of spherulites), the crosslinked elastomer particles enhanced crystal growth rate, reducing the nucleation energy contribution from PP chain folding. Moreover, the crosslinked elastomer particles increased the final thickness of PP lamellae from that of neat PP, and this was corroborated by the XRD results. On comparing the two types of elastomer, it was found that the EOC particles were more effective in heterogeneous cell nucleation than the EPDM particles. The morphological study by SEM revealed completely altered PP spherulite size and shape, as well as their altered distribution, affected by heterogeneous nucleation effects of the crosslinked elastomer particles.

Introduction

Blending of elastomers with semi-crystalline thermoplastics to produce thermoplastic vulcanizates (TPVs) has been motivated by simple fabrication of elastomeric products as an alternative to the conventional manufacture of thermoset elastomers. The TPV's typical phase morphology has micro-dispersed crosslinked elastomer particles in a continuous thermoplastic matrix [1, 2]. Hence, this type of materials combine sufficient functional performance, challenging that of conventional crosslinked elastomers, with fascinating advantages from the ability to be processed as thermoplastics [3, 4]. Dispersion of the crosslinked elastomer phase promotes elasticity and toughness of the TPVs, while the thermoplastic phase offers good melt processability, and also the crystallites in the thermoplastic phase promote the physical and mechanical properties of these blends [5].

Crystallization of a semi-crystalline polymer involves crystal formation by the partial alignment of molecules. The crystallization process consists of three stages [6]. The first stage involves formation of nuclei, termed primary nucleation, and their subsequent growth in the second stage to form crystals, known as secondary nucleation. After the end of secondary nucleation, thickness of the formed lamellar crystals increases along with crystallinity, in this final third stage named secondary crystallization. Crystallization of the thermoplastic in the

✉ Anoma Thitithammawong
anoma.t@psu.ac.th

[1] Department of Rubber Technology and Polymer Science, Faculty of Science and Technology, Prince of Songkla University, Pattani Campus, Pattani 94001, Thailand

[2] Chinese Agricultural Ministry Key Laboratory of Tropical Crop Product Processing, Agricultural Product Processing Research Institute, Chinese Academy of Tropical Agricultural Sciences, Zhanjiang 524001, People's Republic of China

[3] Research and Development Center, Innovation Group (Thailand) Company Limited, Bangkok 10240, Thailand

[4] Faculty of Science and Industrial Technology, Prince of Songkla University, Surat Thani Campus, Surat Thani 84000, Thailand

TPV is a key determinant of the mechanical strength and the processing characteristics of the TPV. It is affected by many factors, for example the chemical structure of the polymer, the molecular weight, the secondary bonding (hydrogen and van der Waals) [7], the crystallization conditions [5, 7–10], and the nucleating agents [11–13]. Incorporation of polymers and fillers can affect the blend properties in two ways. Firstly, the polymers and fillers act as blend components that directly affected strength, stiffness, toughness, adhesion, and abrasion properties [14, 15]. Secondly, they may impede crystallization in the polymer matrix, which consequences to crystallization kinetics, crystallite morphology and size, and degree of crystallinity [14–16]. Our previous work [17] reports an analysis of non-isothermal crystallization of the PP in EPDM/PP and EOC/PP TPVs. The results clearly demonstrate that the dispersed crosslinked elastomer particles in the TPV act as an effective nucleating agent, accelerating crystallization of the semi-crystalline PP phase by reducing required undercooling (ΔT). The acceleration of crystallization reduces energy consumption by crystallization and saves time, providing cost benefits in processing. Furthermore, the crystallization behaviors and melting characteristics of PP as neat and in the TPVs, in relation to the cooling rate, were reported. However, the reduced ΔT affected by the crosslinked elastomer particles, or a rapid cooling rate, may cause bulk crystallization including nucleation and crystal growth, which affect both crystal size and crystallinity obtained [18, 19].

Therefore, in the present an intense effort was made to evaluate the equilibrium melting temperature $\left(T_m^0\right)$ of the PP phase in blends with two crosslinked elastomers, namely ethylene propylene diene terpolymer (EPDM) and ethylene octene copolymer (EOC). Thereafter, the obtained T_m^0s were further related to theoretical models, in order to deeply investigate the whole range of crystallization stages from primary and secondary nucleation to secondary crystallization of PP in the EPDM/PP and the EOC/PP TPVs. Relevant to these aspects, both X-ray diffraction and SEM observations will be discussed.

Experimental section

Materials

Isotactic polypropylene homopolymer (PP, grade HP500N) having a melt flow rate of 12 g/10 min (2.16 kg, 230 °C) and a density of 0.91 g/cm^3 was supplied by HMC Polymer (Thailand). Ethylene propylene diene terpolymer (EPDM, grade JSR EP22) having 4.5% ethylidene norbornene, 54% ethylene content and a density of 0.87 g/cm^3 was manufactured by Japan Synthetic Rubber (Japan). Ethylene octene copolymer (EOC, grade Engage 8003) containing 91.3 mol% ethylene and 9.7 mol% octane, and having a density of 0.89 g/cm^3, was manufactured by Dow Chemical

(USA). Stabilizers (Irganox 1076 and Irgafos 168) were provided by Ciba Specialty Chemicals, Switzerland. Ultrablend 6000 used as homogenizing agent was supplied by Performance Additives, Malaysia. Paraffinic oil (Diana PW90) was supplied by Idemitsu Kosan, Japan. Dicumyl peroxide (DCP, Percumyl D) used as vulcanizing agent was supplied by Chemmin, Thailand. Trimethylolpropane trimethacrylate (TMPTMA, SR350) used as peroxide co-agent was manufactured by Sartomer Asia, China.

Preparation of the samples

Dynamically vulcanized EPDM/PP and EOC/PP blends at the fixed 50/50 parts by weight blend proportions of rubber/thermoplastic were prepared using an internal mixer (Brabender EC plus, Germany). The mixing conditions were set at: initial chamber temperature 170 °C, rotor speed 90 rpm, and 0.9 fill factor. The blend formulation is shown in Table 1. PP was first fed into the mixing chamber and melt mixed for 2 min before addition of the elastomer. The mixing was continued for 3 min and after that a mixture of the stabilizers and the homogenizing agent were incorporated, and mixed for 1 min. Paraffinic oil was separated into two parts and these were stepwise incorporated with 1 min mixing for each. Dynamic vulcanization was performed by adding trimethylolpropane trimethacrylate 0.5 min prior to introducing dicumyl peroxide into the mixture, and mixing for 3.5 min to complete the blend preparation. Prior to testing and characterization, flat sheet TPV specimens with a thickness of 0.2 cm were made by compression molding in a machine equipped with water circulation. The mold temperature was first set at 200 °C and then cooled to ambient temperature at a cooling rate of approximately 25 °C/min.

Characterizations

Differential scanning calorimetry (DSC)

Isothermal crystallization and subsequent melting were performed in a differential scanning calorimeter (DSC, Q2000, TA Instrument, USA) under nitrogen atmosphere.

Table 1   Blend formulation

Chemicals	Relative amount by weight
PP	50
EPDM or EOC	50
Homogenizing agent	1
Stabilizers	1
Paraffinic oil	10
TMPTMA	1
DCP	2

Approximately 5 mg of a sample was sealed in an aluminum pan, and first heated from 40 °C to 200 °C at a heating rate of 40 °C/min, and then held at this temperature for 5 min in order to erase effects of thermal history. Then isothermal crystallization was induced by rapid cooling of the sample from 200 °C to the designated isothermal crystallization temperature (T_c), i.e., 122, 124, 126, 128 and 130 °C, at a cooling rate of 40 °C/min. The sample was isothermally crystallized at the designated T_c for 30 min, to reach sufficient crystallinity prior to re-heating at 10 °C/min to determine the melting temperature and heat of fusion. Time profiles of temperature used in the test are summarized in Fig. 1.

X-ray diffraction (XRD)

An X-ray diffractometer (Philips Generator TW1830, The Netherlands) was used to establish the crystallinity characteristics of the samples. The test was performed at 15 kV and 5 mA with monochromatized CuKα radiation with a graphite sample monochromator (wavelength λ = 0.154 nm). The diffractograms were scanned over the 2θ range of 10–30 degrees, with a scanning rate of 1.0°/min.

Scanning electron microscopy (SEM)

An FEI Quanta-200 scanning electron microscope (SEM) (FEI, Czech Republic) was used to investigate morphology of the crystalline phase in the TPVs. The cryogenically fractured specimen was etched with a mixed etchant to remove the amorphous phase, according to the procedure developed by Olley and Basset [20]. The etchant was composed of 3 wt% potassium permanganate ($KMnO_4$), 65 wt% concentrated sulfuric acid (H_2SO_4), and 32 wt% concentrated phosphoric acid (H_3PO_4). To achieve the optimum etching conditions, experiments were performed with varied etching times (i.e., 2 and

4 h). After etching, the specimens were first washed with 12.5 wt% sulfuric acid solution in water, and subsequently ultrasonicated using an Omni Ruptor 400 W ultrasonic homogenizer (Omni international, USA) at 20 kHz, in distilled water for 1 min. Gold was sputter coated onto the dry-etched surface before visualization with the SEM, used in the secondary electron (SE) mode.

Results and discussion

Melting characteristics of isothermally crystallized samples and their equilibrium melting temperatures

The key parameter of interest is the equilibrium melting temperature $\left(T_m^0\right)$, which is defined as the melting temperature of a perfect crystal formed by an extended chain. The T_m^0 is important factor for adjusting the cooling conditions, in order to achieve the desired crystalline characteristics in a semicrystalline polymer. Moreover, it is a necessary parameter in several theories of nucleation and crystallization kinetics. In order to estimate the T_m^0s of the crystallizable polymers, isothermal crystallization experiments were performed using a DSC, and the designated crystallization temperatures (T_c) were set in the temperature range from a typical melting temperature (T_m) to the glass transition temperature (T_g) of PP. Fig. 2 shows melting endotherms obtained with the fixed 10 °C/min heating rate, of the isothermally crystallized EPDM/PP blends at the designated T_cs from 122 to 130 °C. The T_m can be directly obtained at the maximum melting peak of an isothermally crystallized sample, as indicated by the dotted line in Fig. 2. It can be seen that the melting peak markedly shifted towards higher temperatures as T_c increased. Similar behavior was also observed in the other investigated
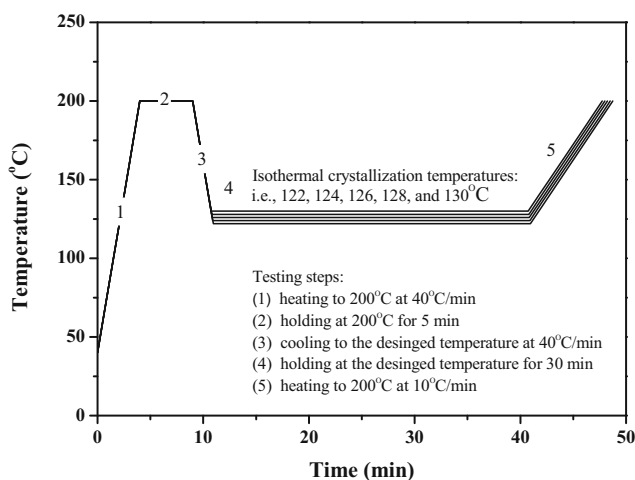
Fig. 1 Time-profiles of temperature used in the isothermal crystallization test
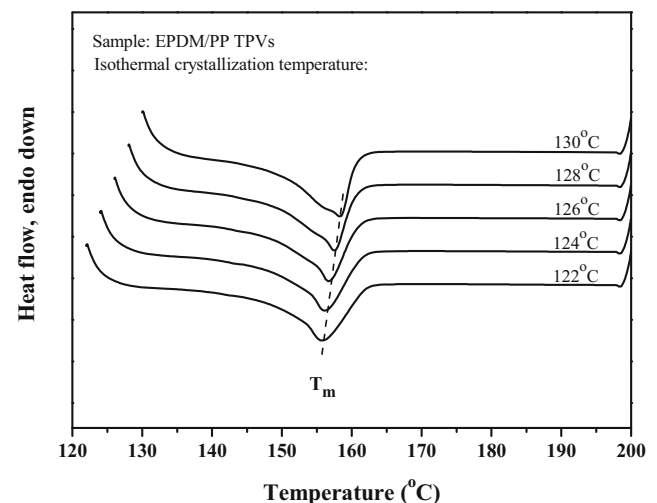
Fig. 2 DSC endothermic thermograms of the EPDM/PP TPVs for various isothermal crystallization temperatures
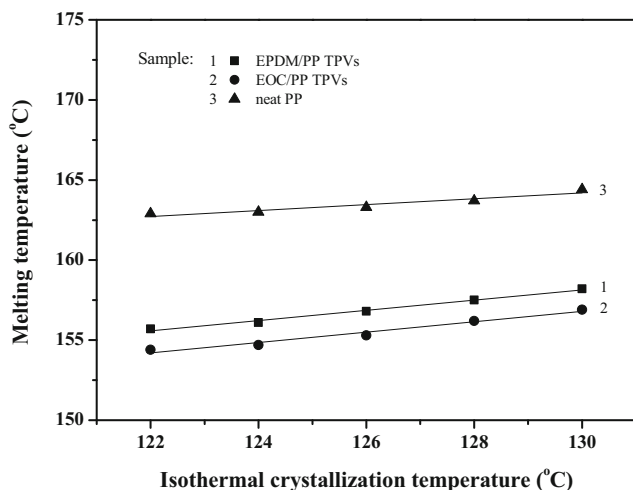
samples, i.e., the neat PP and the EOC/PP TPVs, as shown in Fig. 3. A higher melting temperature indicates more perfect PP crystals [21, 22].

Irrespective of the T_c, in Fig. 3 a significant decrease in T_m is found for both the EPDM/PP and the EOC/PP TPVs relatively to that of the neat PP. The EPDM/PP TPVs exhibit a few degrees higher T_m than the EOC/PP TPVs. The variation in T_m of the PP phase in the blend was related to the dispersed elastomer particles in the PP matrix. The melting of small or imperfect PP crystals tended to happen at a lower temperature than the melting of a typical PP crystal [17]. The Hoffman-Weeks [11] method is a common approach in relevant publications [23–26] for estimating T_m^0 from experimental data on isothermal crystallization. The Hoffman-Weeks approach uses the linear approximation:
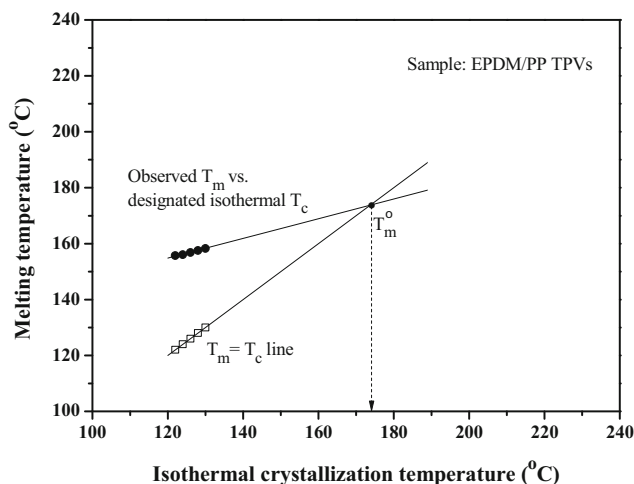
$$T_m = T_m^0 \left[1 - \frac{1}{\beta} \right] + \frac{T_c}{\beta} \qquad (1)$$

where T_m denotes the melting temperature of crystals formed at a certain isothermal crystallization temperature (T_c). T_m^0 is the equilibrium melting temperature, and β is the lamellar thickening coefficient that is the ratio of lamellar thicknesses (l_c/l_0), with final lamellar thickness (l_c) and initial lamellar thickness (l_0). Note that the lamellar thickening coefficient and the thicknesses of the lamellae can be estimated from temperature data during cooling and melting, which will be discussed in Crystalline morphology associated with secondary crystallization Section.

Fig. 4 shows the linear model according to the Hoffman-Weeks theory, fit to experimentally observed T_ms of the EPDM/PP TPVs at the various designated isothermal T_cs, and extrapolated up to $T_m = T_c$. The results across the various samples are summarized in Table 2. The T_m^0 of neat PP is

Fig. 4 Determination of T_m^0 for PP in the EPDM/PP TPVs, according to the Hoffman-Weeks approach

approximately 180 °C which is about 5 degrees lower than the reported value in literatures [27–29]. While, the PP in EPDM/PP and EOC/PP TPVs has lower T_m^0s of about 174 and 172 °C, respectively. Decrease of the T_m^0 for the PP matrix in EPDM/PP and EOC/PP TPVs was caused by the elastomer phase. The elastomer particles affected the PP chain's crystallinity, acting as chain defects that interrupted the chain regularity, and thereby lowering T_m^0.

Non-isothermal crystallization characteristics

To further evaluate the effects of crosslinked EPDM and EOC particles on PP crystallization, non-isothermal crystallization conditions close to the practical molding in industrial processing were investigated. The schematic DSC profile in Fig. 5 represents non-isothermal crystallization of a polymer, divided into three regimes, namely Regime I: primary nucleation, Regime II: secondary nucleation, and Regime III: secondary crystallization. Table 3 summarizes the non-isothermal crystallization characteristics of the samples at various cooling rates.

Irrespective to the sample type, it can be seen in Fig. 5 and Table 3 that $T_{c,onset}$ shifted toward lower temperatures when the cooling rate was faster, because then less time was available to initiate the nuclei. Typically, the nucleation rate is low at high temperatures. Therefore, under fast cooling a polymer can crystallize later than expected. A faster cooling rate

Fig. 3 Melting temperatures of isothermally crystallized samples at various isothermal crystallization temperatures

Table 2 Equilibrium melting temperatures $\left(T_m^0 \right)$ of the investigated samples, according to the Hoffman-Weeks approach

Samples	EPDM/PP	EOC/PP	neat PP
T_m^0 (°C)	173.6	171.6	179.8
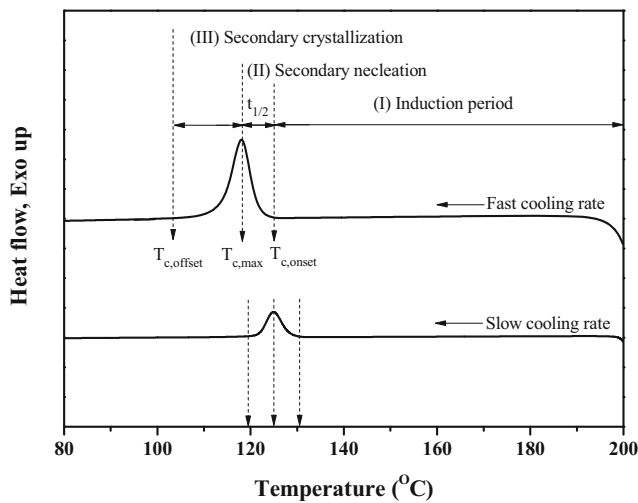
Fig. 5 Schematic illustration of the effects of cooling rate on crystallization

eventually provides a high nucleation rate with reduced crystallization induction time (t_i) of primary nucleation (Regime I). The t_i is related to the amount of time required by initiation of a stable nucleus. It corresponds to the time elapsed from the temperature setting in the process to $T_{c,onset}$ when nuclei are first detected. Analysis in this regime will be detailed in Primary nucleation and its relation to nucleation barrier and activity Section.

After the stable nuclei are created during Regime I, growth of new layer of polymer crystals on the original primary nuclei occurs, and this is called secondary nucleation (crystal growth). During this stage, the exothermic enthalpy peak of crystallization spontaneously increases to reach its maximum at $T_{c,max}$, indicating the end of secondary nucleation. The time taken in this state is called the half-time of crystallization ($t_{1/2}$), and is obtained from the temperature difference divided by cooling rate ($t_{1/2} = [T_{c,onset} - T_{c,max}]/\varphi$). This is directly related to the secondary nucleation rate or the growth rate ($G = 1/t_{1/2}$) [25, 26]. As mentioned above, upon increasing the cooling rate, there is less time available for the PP molecules to orient and form crystals, leading to reduced temperature during crystallization of the PP (see decreasing trend of $T_{c,onset}$ in Table 3). Crystallization is temperature dependent, and the growth rate of crystallization is typically suppressed at a low temperature. That is why the $t_{1/2}$ obviously decreases with the cooling rate. Lauritzen–Hoffman theory will be adopted to analyze the secondary nucleation (Regime II) in the present work; the details are discussed in Secondary nucleation (spherulite growth) analysis by Lauritzen–Hoffman theory Section.

The crystallization does not stop with the growth of crystals, instead secondary crystallization continuously proceeds in Regime III (see Fig. 5). During secondary crystallization after the half-time of crystallization up to the offset of crystallization ($T_{c,offset}$), there is continuous increase in crystallinity and in thickness of the already formed lamellar crystals. The analyses of crystalline morphology, including their lamellar thickness, and the lamellar thickening coefficient in theoretical crystallization models, will be discussed in Crystalline morphology associated with secondary crystallization Section.

Primary nucleation and its relation to nucleation barrier and activity

Primary nucleation is the first step in crystallization. It is simply defined as formation of the initial nuclei. Classical nucleation theory [12] is the most common theoretical model used for the induction time:

$$\Delta G = \left[\frac{16\pi (\gamma_{SL})^3 (T_m^0)^2}{3 (\Delta H_f)^2} \right] \frac{1}{\Delta T} \qquad (2)$$

where ΔG represents the nucleation energy barrier. ΔH_f is the heat of fusion, and γ_{SL} is the interfacial energy at the solid-liquid interfaces of the nuclei. T_m^0 is the equilibrium melting temperature, and ΔT is the degree of undercooling that is defined as the difference between T_m^0 and the crystallization temperature (T_c).

According to Eq. (2), as ΔT increases the nucleation energy barrier (ΔG) decreases, so nucleation becomes easier. In addition, ΔG can also be reduced by an effective nucleating

Table 3 Crystallization and melting characteristics of PP as neat or in the TPVs at various cooling rates

Samples	φ (°C/min)	$T_{c,onset}$ (°C)	$T_{c,max}$ (°C)	T_m (°C)	$t_{1/2}$ (s)	ΔT (°C)	t_i (s)
neat PP	5	126.8	114.1	162.0	152	65.7	878
	10	124.4	111.3	161.2	78	68.5	454
	15	123.0	109.7	160.5	53	70.1	308
	20	122.0	108.6	159.8	40	71.2	234
	25	121.2	107.7	159.0	30	72.1	189
EPDM/PP	5	132.3	124.8	157.1	91	48.8	812
	10	129.3	121.4	156.2	47	52.2	424
	15	127.5	119.5	155.7	32	54.1	290
	20	126.2	118.2	155.3	24	55.4	221
	25	125.3	117.2	155.0	20	56.4	179
EOC/PP	5	131.0	124.4	155.3	79	47.2	828
	10	127.9	121.3	154.5	40	50.3	433
	15	126.1	119.5	154.0	27	52.1	296
	20	124.8	118.2	153.6	20	53.4	226
	25	123.8	117.2	153.3	16	54.4	183

agent incorporated into the molten polymer mix. The free energy barrier for heterogeneous nucleation (ΔG_{hetero}) is given by:

$$\Delta G_{hetero} = \Delta G_{homo} \times f(\theta) \tag{3}$$

where ΔG_{homo} is the free energy barrier for homogeneous nucleation and f(θ) stands for a geometric factor that depends on the contact angle of the existing and the forming phases, given by:

$$f(\theta) = \frac{(2 + cos\theta)(1 - cos\theta)^2}{4} \tag{4}$$

Note that if θ < 180, then the value of f(θ) is smaller than 1, which lowers ΔG_{hetero} of heterogeneous nucleation. The difference in the nature of homogeneous and heterogeneous nucleation can imply significant energetic differences. As expected, the presence of dispersed crosslinked EPDM or EOC particles in the PP matrix, which act as nucleating agents accelerating PP crystallization, minimizes the first term (ΔG_{homo}) in Eq. (3) by lowering ΔT. Furthermore, the crosslinked EPDM and EOC particles that are relatively small-sized (about 0.2–0.5 μm) with low interfacial tension (high wetting) against the PP matrix [30], will also tend to reduce the second factor f(θ) in Eq. (3). The contact angle of the PP matrix against the crosslinked elastomer particles can be estimated from the surface free energies by Young's eq. [31]:

$$\gamma_S = \gamma_{S/L} + \gamma_L cos\theta \tag{5}$$

$$cos\theta = \frac{\gamma_S - \gamma_{S/L}}{\gamma_L} \tag{6}$$

where, γ_S and γ_L are the surface tensions (energies per unit area) of the solid and the liquid, respectively. $\gamma_{S/L}$ is the interfacial tension at the solid-liquid interface, and θ is the contact angle of the liquid on the solid surface.

In the present work, the contact angles of PP on EPDM and EOC surfaces were estimated from surface tensions of the neat materials at 180 °C [30]. By using these data in Young's equation, it was found that PP exhibits a relatively higher contact angle with EPDM surface (i.e., 47.9°) than with EOC surface (i.e., 21.7°). The calculated f(θ) for the EPDM/PP and EOC/PP systems is given in Table 4. It can be concluded from the f(θ) values that the free energy barrier for heterogeneous nucleation of PP (ΔG_{hetero}) should decrease when EPDM or

Table 4 Contact angle (θ) and geometric factor (f(θ)) for PP on EPDM or on EOC, and nucleation activity (φ) on PP by EPDM or EOC

Characteristics	EPDM/PP	EOC/PP
θ (°)	47.9	21.7
f(θ)	0.073	0.004
φ	0.37	0.35

EOC was introduced, and EOC showed a greater effect on heterogeneous nucleation than EPDM. In the present work, however, the estimates of f(θ) are rough. We should rather use the surface tension of the crosslinked elastomer and the molten thermoplastic at the certain T_c. Unfortunately, due to limitations of these experiments, the values of ΔG_{hetero} at given values of T_c cannot be obtained. However, nucleation will be discussed in terms of the nucleation activity (φ).

A method to estimate the nucleation activity of a polymer melt has been proposed by Dobreva and Gutzow [32, 33]. The nucleation activity is a measurement of the work decrement of three-dimensional nucleation with the addition of a foreign substrate. Typically, the values of φ is in a ranges from 0 to 1. The stronger the activity of the foreign substrates, the lower the φ value should be. The equations describing this approach are as follows:

$$\phi = B_{hetero} \Big/ B_{homo} \tag{7}$$

where B is a nucleation parameter of heterogeneous nucleation (B_{hetero}) or homogeneous nucleation (B_{homo}). It can be calculated as follows:

$$B = \frac{\omega\sigma^3(V_m)^2}{3nk_B T_m^0(\Delta S_m)^2} \tag{8}$$

where ω is a geometric factor, σ is the specific energy, V_m is the molar volume of the substance, n is the Avrami index, k_B is the Boltzmann constant, ΔS_m is the entropy of melting, and T_m^0 is the equilibrium melting temperature.

Furthermore, B can also be determined experimentally from the slope of Eq. (9), by plotting ln φ against the inverse squared under cooling $1/\Delta T^2$.

$$ln\varphi = constant - \frac{B}{\Delta T^2} \tag{9}$$

Plots of ln φ against $1/\Delta T^2$ for the neat PP and the blends are shown in Fig. 6. The slopes of the fitted lines reveal the values of B_{homo} for neat PP and B_{hetero} for EPDM/PP or EOC/PP TPV. The values of φ calculated from Eqs. (7) and (9) for
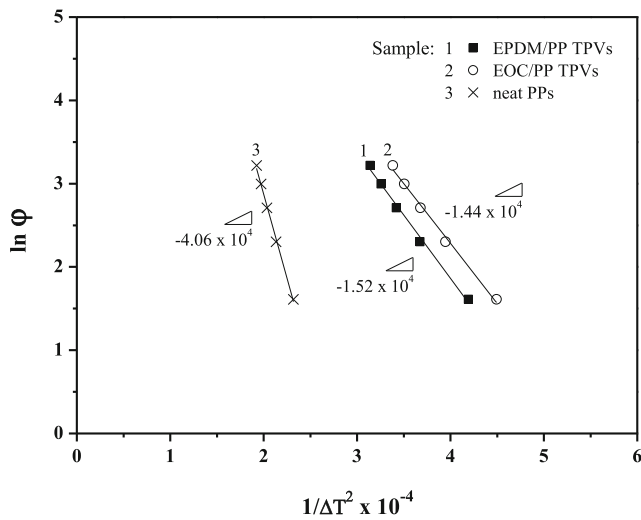
Fig. 6 Analysis of nucleation activity following the approach of Dobreva and Gutzow

EPDM/PP and EOC/PP TPVs are given in Table 4. It is noticed that the ϕ values for EPDM/PP and EOC/PP TPVs were less than 1, indicating that the crosslinked EPDM and EOC particles were efficient nucleating agents providing nucleation sites, which can increase crystallization rate of the PP matrix. This relates well to the observed decrease in t_i of PP crystallization in the TPVs, when compared to that in the neat PP, at a given cooling rate (see Table 3). Moreover, the EOC/PP TPV had lower ϕ and thereby slightly higher nucleation effect than the EPDM/PP TPV, as also seen in the shorter $t_{1/2}$ and lower $T_{c,onset}$ and $T_{c,max}$ in Table 3. On comparing to other filled PPs, SiO_2 and Si_3N_4 particles had a ϕ value of about 0.85 in PP, at 5% loading level [34, 35]. In PP filled with 1% multiwall carbon nanotubes or 2% talc, the values of ϕ were 0.50 and 0.56, respectively [36, 37]. It is obvious that the crosslinked EPDM and EOC particles had comparatively small ϕ values. This confirms that the crosslinked EPDM and EOC particles are effective nucleating agents for PP, in comparison to more commonly used/studied fillers [34–37].

Secondary nucleation (spherulite growth) analysis by Lauritzen–Hoffman theory

The Lauritzen–Hoffman theory assumes that the free energy barrier to nucleation has an energetic origin, and provides a general expression for the growth rate (G) of a linear polymer crystal with folded chains:

$$G = G_0 \exp\left[-\frac{U^*}{R(T_c - T_\infty)}\right] \exp\left[-\frac{K_g}{f T_c \Delta T}\right] \tag{10}$$

$$f = \frac{2T_c}{T_m^0 + T_c} \tag{11}$$

where G_0 is a constant parameter, U^* is the diffusional activation energy for the transport of crystallizable segments at the liquid-solid interface (usually set equal to 6280 J/mol), R is the universal gas constant, T_c is the crystallization temperature, T_∞ is the hypothetical temperature below which there is no chain motion (usually taken as $T_\infty = T_g - 30$), T_g is the glass transition temperature of PP (taken as 10 °C for this study), K_g is the nucleation constant, which can be related to the product of lateral and fold surface free energies, f is a correction factor that takes into account variations in bulk melting with temperature as given in Equation (11), T_m^0 is the equilibrium melting temperature, and ΔT is the undercooling. The growth rate of crystallization (G) can be approximated by the reciprocal of half-time of crystallization ($G = 1/t_{1/2}$), and then Equation (10) can be logarithmically transformed and rearranged as follows:

$$\ln\left[\frac{1}{t_{1/2}}\right] + \frac{U^*}{R(T_c - T_\infty)} = \ln G_0 - \frac{K_g}{f T_c \Delta T} \tag{12}$$

According to Eq. (12), a plot of the left-hand side against $1/(fT_c\Delta T)$ should yield a straight line with the intercept $\ln G_0$ and the slope $-K_g$.

As decribed in Primary nucleation and its relation to nucleation barrier and activity Section, the crosslinked EPDM and EOC particles act as heterogeneous nucleating agent in the crystallization of PP, and accelerate the rate of crystallization. In order to well understand the crystallization stage, the secondary nucleation (Regime II in Fig. 5) was investigated using data from the non-isothermal crystallization of PP in neat form and in the EPDM/PP and EOC/PP TPVs, given in Table 3. The Lauritzen–Hoffman equation which is originally used for isothermal crystallization has been adopted in the study of non-isothermal crystallization by using the following relationship:

$$t = \frac{T_0 - T_c}{\alpha} \tag{13}$$

where t is the total crystallization time, T_0 is the onset temperature of crystallization, T_C is the crystallization temperature and α is the cooling rate. Thus, Eq. (12) can be transformed into following equation [38–40]:

$$\ln\left[\frac{1}{t_{1/2}}\right] + \frac{U^*}{R(T_0 - \alpha t - T_\infty)} = \ln G_0 - \frac{K_g}{f(T_0 - \alpha t)\Delta T} \tag{14}$$

Fig. 7 shows such crystal growth analysis of the non-isothermal crystallization according to the modified
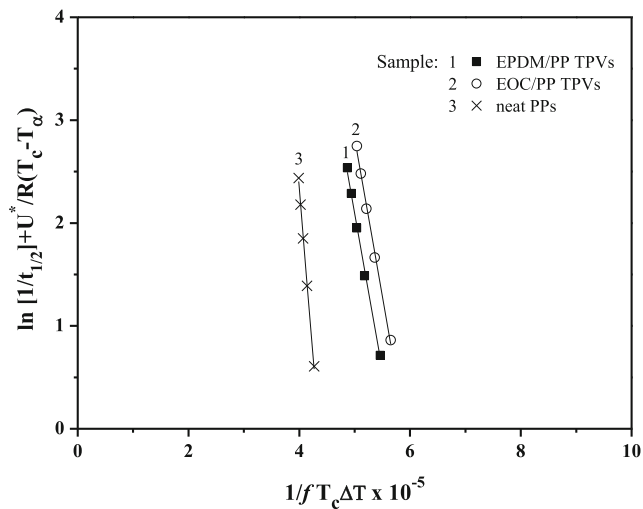
Fig. 7 Estimation of secondary nucleation rate in accordance with the Lauritzen–Hoffman theory

Lauritzen–Hoffman theory. The nucleation constants K_g are listed in Table 5. In fact, an effective nucleating agent should reduce K_g [41]. According to prior literature [42] the effect of surface-treated SiO_2 on the K_g of PP is to decrease it almost linearly with the loading level of SiO_2. This phenomenon was also observed in PP filled with carbon nanotubes [43], with talc [44] and with polybutadiene rubber [26]. As seen in Table 5, the incorporation of crosslinked EPDM and EOC particles into the PP matrix caused a sharp decrease in K_g relative to the neat PP. This might be explained by enhanced interfacial interactions in EPDM/PP and EOC/PP. EPDM and EOC have functional groups with affinity to both polar and non-polar components in PP, and hence act as good binding material [30]. Enhanced EPDM/PP and EOC/PP interfacial interactions may decrease the energy required to fold PP chains during secondary nucleation. This again confirms that nucleation of the PP is influenced by the presence of crosslinked EPDM and EOC particles.

Crystalline morphology associated with secondary crystallization

The crystal structures are largely lamellar with folded chains. These lamellar structures generally contain also amorphous parts that pass from one crystalline region to the next. Thickening of the lamellae occurs after the secondary nucleation regime (Regime II), and crystalline lamellae with a certain thickness are finally obtained by the secondary

Table 5 Secondary nucleation constants of the investigated samples according to the modified Lauritzen–Hoffman equation

Samples	EPDM/PP	EOC/PP	neat PP
$K_g \times 10^5$	4.01	4.03	5.47

crystallization (Regime III). As thickness of the lamellae strongly affects mechanical and thermal properties of a semi-crystalline polymer, the study of crystallinity is very relevant. Hoffman-Weeks [11] and Thomson-Gibbs [45] equations are well-known theoretical models relating the lamellar characteristics to the thermal characteristics. In the present study, the initial lamellar thickness (l_0), the final lamellar thickness (l_c), and the lamellar thickening coefficient (β) were evaluated from a mathematical model:

$$l_c = l_0 \beta \tag{15}$$

where β for a crystallizable polymer can be estimated by fitting its thermal characteristics with the Hoffman-Weeks equation, as given in Eq. (1).

Thomson and Gibbs model describes the temperature dependence of the final lamellar thickness l_c:

$$T_m = T_m^0 \left[1 - \frac{2\sigma_\theta}{l_c \Delta H_f \rho_c} \right] \tag{16}$$

where T_m^0 is the equilibrium melting temperature, σ_θ is the fold surface free energy, ΔH_f is the equilibrium melting enthalpy, and ρ_c is the density. The following values were literature curated for PP: $\sigma_\theta = 100 \times 10^{-7}$ J/cm^2 [46, 47], $\Delta H_f = 209$ J/g [5], and $\rho_c = 0.91$ g/cm^3.

Fig. 8 represents the effects of cooling rate on the lamellar characteristics of PP in EPDM/PP TPVs. It can be seen that l_0, which refers to thickness of the formed lamellae at start of the secondary crystallization, strongly depended on the cooling rate, continually decreasing with the cooling rate. This is in accordance to several prior studies [48–50] that have found with large ΔT (see Table 3, the ΔT is found to increase with cooling rate) and rapid quenching that a large number of small
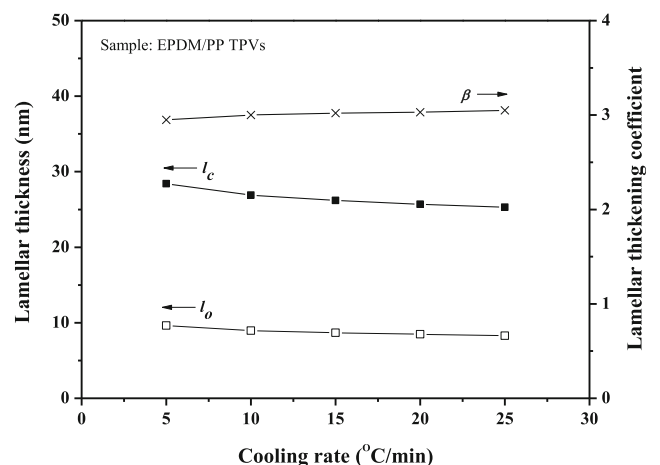
Fig. 8 Lamellar thickness and lamellar thickening coefficient of PP in the EPDM/PP TPVs as functions of cooling rate

nuclei (high nucleation density) were obtained. At a given cooling rate, the PP lamellae in EPDM/PP TPVs had initial thicknesses (l_0) in the range 8–10 nm, and reached final thicknesses (l_c) of about 25–28 nm. During the secondary crystallization of PP in the EPDM/PP TPVs, the PP lamellae had lamellar thickening coefficient (β) of approximately 3, indicating that the PP lamellae got about three-fold thicker. However, it should be noted that lamellar thickness evaluated from DSC result are inadequate unless the precise thermodynamic data (fold surface free energy, crystal density and 100% crystal heat of fusion) obtained from small-angle X-ray scattering (SAXS) are incorporated for discussion.

The effects of crosslinked elastomer particles in the PP matrix on PP lamellar characteristics are shown in Fig. 9. The lamellar characteristics of PP in all investigated samples (i.e., neat PP, EPDM/PP TPVs, and EOC/PP TPVs) were obtained at the fixed 25 °C/min cooling rate. It is seen that l_0 and l_c of PP in both EPDM/PP and EOC/PP TPVs were clearly higher than those of the neat PP. This is due to effects of the crosslinked elastomers as nucleating agents [26, 51]. Lamellar thickening as well as crystalline perfection depends on chain mobility via translational diffusion within the crystalline phase [52]. In the presence of crosslinked elastomer particles, the T_c of PP in the TPVs was increased. This may indicate that the chain mobility or the chain diffusion of PP was enhanced. However, the neat PP exhibited higher β than the PP in EPDM/PP or in EOC/PP TPV. The neat PP lamellae thickened by approximately 3.5 fold during secondary crystallization, where in the EPDM/PP or the EOC/PP TPV the thickening was about 3 fold. The observations indicate that the crosslinked elastomer particles as heterogeneous nucleating agents provided the TPVs with thicker PP lamellae.

To further clarify the character of secondary crystallization of PP, crystallographic structures of the PP phases in the

EPDM/PP and the EOC/PP TPVs were also investigated by X-ray diffraction, and compared with neat PP. Crystal cell size (l_{110}) values of α-form PP were roughly derived using the Scherrer equation [26], and also the Bragg spacing (d_{110}, the interplanar distance between consecutive (110) planes) was evaluated by means of Bragg's law [53]. The determinations by X-ray diffraction are summarized in Table 6. The d_{110} and l_{110} values suggest that the crosslinked elastomer particles not only promoted such PP phase that had similar unit cell as the neat PP, but also increased the spacing in monoclinic α-form crystals. The crystal lattice spacing in monoclinic α-form in the EOC/PP TPV was larger than in the EPDM/PP TPV. This observation is in agreement with the increased l_0 and l_c in the DSC measurement, as previously discussed in relation to Fig. 9. The crosslinked elastomer particles may affect the crystal size in the PP matrix by various mechanisms or distinct effects. These include (1) the nucleation effect, (2) the crystal growth process, and (3) the steric hindrance factor [14]. The increase in l_{110} crystal lattice spacing of PP with the addition of vulcanized elastomers might be attributed to both the nucleation effect and the crystal growth process. The crosslinked elastomer particles caused the EPDM/PP and the EOC/PP TPV to have relatively high T_c values (see Table 3), by acting as heterogeneous nucleating agents that accelerated crystallization of the PP. After some nuclei had been created, the crystal growth followed simultaneously with further nucleation.

When ΔT is small (low cooling rate), the crystal growth rate is moderate, and the lamellar thickness in crystals produced is greater [48–50]. The rank order of observed ΔT was EOC/PP TPV < EPDM/PP TPV < neat PP when compared at a fixed cooling rate, and this matches well the lamellar thicknesses: the l_{110} crystal lattice spacing of PP in the EPDM/PP and in the EOC/PP TPVs was larger than in the neat PP. The values l_c of crystalline size in all investigated samples, obtained from the Thomson-Gibbs equation, are also summarized in Table 6 for comparison. It is noted that the l_c were nearly similar to the l_{110} obtained from the Scherrer equation using X-ray diffraction measurements. This confirms that an analysis of the secondary crystallization kinetics by DSC measurements was reliable. Furthermore, it is found that the d_{110} spacing obtained from Bragg's equation was comparable across all samples, indicating similar interplanar distances of
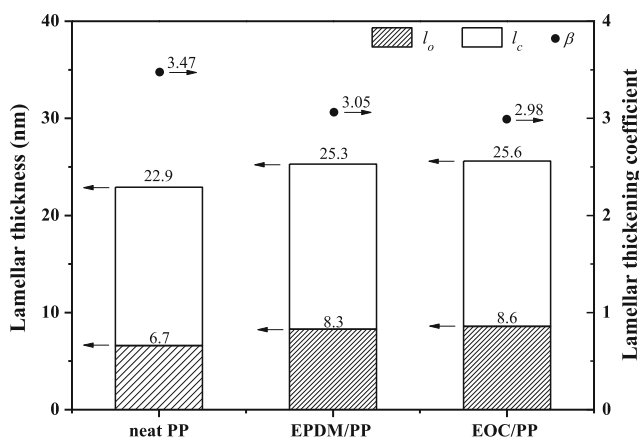
Fig. 9 Lamellar thickness and lamellar thickening coefficient of PP as neat and in the EPDM/PP and the EOC/PP TPV, at the fixed 25 °C/min cooling rate

Table 6 Lamellar thicknesses derived from X-ray diffraction in crystallized samples, along with estimates obtained from DSC measurements
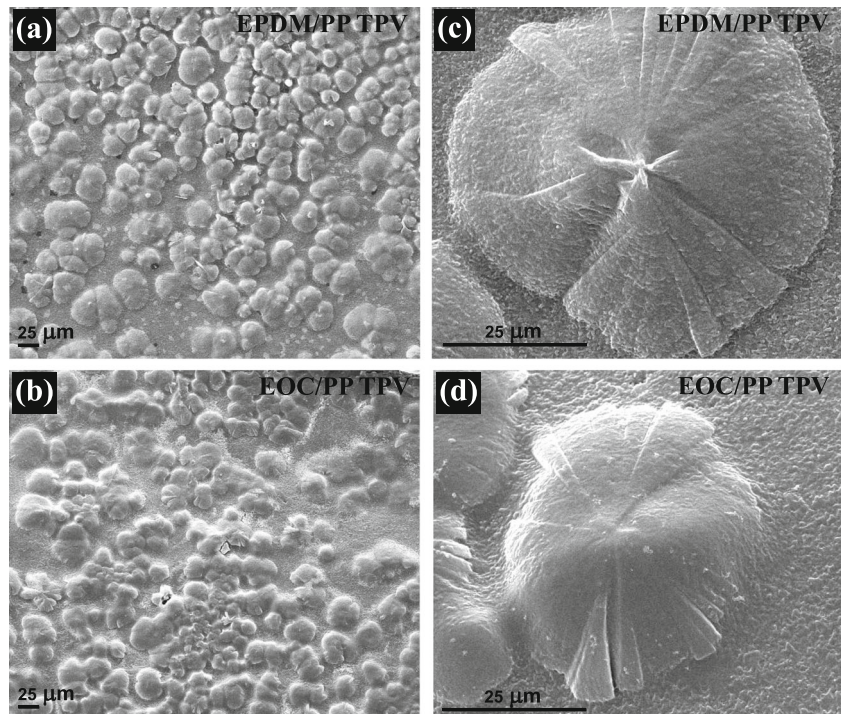
Samples	d_{110} (nm)	l_{110} (nm)	$l_{c,DSC}$ (nm)
neat PP	6.27	23.4	22.9
EPDM/PP	6.31	24.1	25.3
EOC/PP	6.31	26.6	25.6
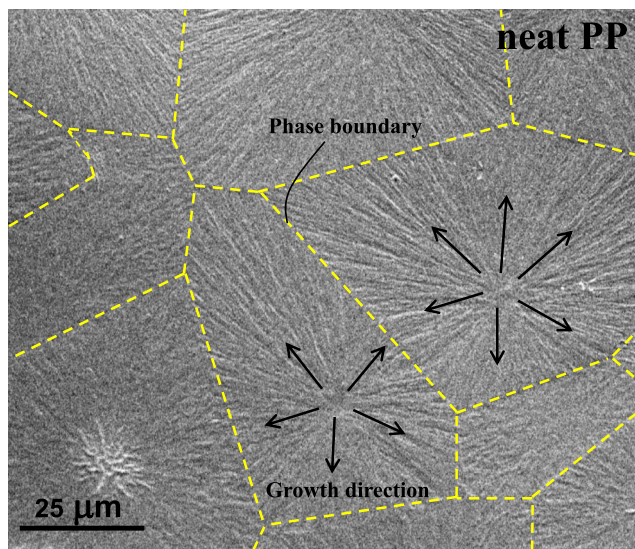
Fig. 10 SE-SEM image of the crystalline phase in neat PP after chemical etching for 4 h (at 1,000× magnification)

SEM observations of crystalline morphology

Spherulite is a typical microstructure of polymer crystals with highly ordered lamellae. During the growth of a crystal (secondary nucleation, Regime II), the polymer chains fold together and then form ordered regions or lamellae, and these grow and expand spherically outwards from the initiating nucleus. To gain further insights into the crosslinked elastomer particles in the thermoplastic matrix, the crystalline structures of the PP phase in the EPDM/PP and the EOC/PP TPV were observed by SEM and compared to those in the neat PP. Non-isothermal crystallization was induced in the fabricated samples by cooling at about 25 °C/min, and the sample surfaces were etched with permanganic acid before imaging with SEM. In permanganic acid etching, the amorphous component is degraded more readily by the active species than the crystalline component. The crystallized form is densely packed and more stable with comparatively strong van der Waals attractions between molecules. Therefore, the crystals would require longer etching time to diffuse and react than the amorphous part [54]. With an appropriate choice of etching time, therefore, the fine details of crystalline structure in the semi-crystalline polymers will appear at the sample surfaces.

consecutive (110) planes. Thickness of the amorphous part between two consecutive planes can be estimated from d_{110} and l_{110}, by subtracting the latter from the former. These estimates of amorphous layer thickness were 38.7, 36.5, and 39.7 nm, for the EPDM/PP, the EOC/PP TPVs, and the neat PP, respectively. This analysis of amorphous layer thickness in the TPVs leads to the conclusion that the crosslinked elastomer particles of about 0.2–0.5 μm size [27] cannot be embedded between two neighboring lamellae, while they may be interspersed between stacks of lamellae.

Fig. 10 shows the crystalline morphology of neat PP etched with permanganic acid solution for 4 h. The arrows indicated the radial growth direction of lamellae outwards from a center, and the phase boundaries between spherulites were formed when they eventually impinge upon each other due to growth: these are shown with a dashed line. Well-developed spherulites about 70 μm in diameter with clear boundaries were

Fig. 11 SE-SEM images of crystallized samples after chemical etching for 2 h, showing the distribution of spherulites in **a** EPDM/PP, and **b** EOC/PP TPVs (at 250× magnification), and detailing spherulite structure in **c** EPDM/PP, and **d** EOC/PP TPVs (at 1,800× magnification)

observed in the neat PP. The spherulites contained straight lamellae and kept growing until further expansion was blocked by other spherulites. Fig. 11 shows the crystalline morphologies of the EPDM/PP and the EOC/PP TPVs, etched in permanganic acid for 2 h. Figs. 11a and b, represent the spherulite formations in the EPDM/PP and the EOC/PP TPV at 250 fold magnification. It can be seen that the spherulites were totally different from those in the neat PP; they were diverse in size and poorly distributed. Some spherulites were connected to each other, but some remain separated. It was found that both the TPVs had smaller sized spherulites, more spherical in shape, than those in the neat PP (see Fig. 10). Moreover, it seems like the EPDM/PP and EOC/PP TPVs had more spherulites than the neat PP per unit area on the surfaces. In fact, the size and number of spherulites are related, as these are both controlled by several parameters such as the structure of the polymer molecules (mobility of the crystallized polymer chain), processing conditions, an intentional addition of nucleating agents (enhancing a number of nucleation sites), etc. [7–10]. In the present work, the TPVs had smaller and more numerous spherulites than the neat PP, because the dispersed crosslinked elastomer particles acted as heterogeneous nucleating agents in the PP matrix. Even though the crosslinked elastomer particles induced reduced ΔT and elevated growth rate ($1/t_{1/2}$) of crystals, the nucleation effects were dominant. The dispersed crosslinked elastomer particles in the TPVs created a large number of nucleation sites, which directly caused a numerous spherulite population (see the nucleation barrier and activity in Primary nucleation and its relation to nucleation barrier and activity Section). This limited the growth space per one spherulite and hence their comparatively small size. Moreover, the crosslinked elastomer particles can generally pass into the inter- and intra-spherulitic regions in the crystalline component of the thermoplastic phase [55]. Crosslinked EPDM and EOC particles may have been trapped inside the PP spherulites, causing irregular geometry that suppresses the mobility of the molecular chains and thereby hinders crystallization: consequently the size of spherulites can also be reduced by this mechanism. Fig. 11c and d are high magnification images of PP spherulite morphology in the EPDM/PP and in the EOC/PP TPV, respectively. These PP spherulites observed were swollen with slightly rough surfaces. The swelling was caused by the etching reagent when the amorphous phase contributes a large fraction of the composition.

Conclusions

The effects of crosslinked EPDM and EOC particles on the whole crystallization process of PP in EPDM/PP and EOC/PP TPVs were assessed. The results confirm that crosslinked elastomer particles caused heterogeneous nucleation of the PP in TPVs, and directly impacted the PP crystallization process. In the early stage of crystallization, the crosslinked elastomer particles promoted shorter primary nucleation time along with lower nucleation activity (ϕ values) of PP in the TPVs than in the neat PP, indicating the particles had strong nucleation effects. Moreover, the crosslinked elastomer particles provided the PP with higher crystal growth rate together with reduced nucleation constant in the secondary nucleation regime. This indicated decreased energy barrier for the PP chain segments to attach to the nucleus, curing crystal growth in the presence of the crosslinked elastomers. In the final regime of secondary crystallization, the crosslinked elastomer particles induced increased lamellar thickness in the PP matrix, relative to that in the neat PP. The morphological study revealed strong obvious effects on the size and shape of PP spherulites that were smaller and poorly distributed in the TPVs. The smaller size was due to the dominant heterogeneous nucleation effects of the crosslinked elastomer particles, increasing numerosity of the crystal population and reducing the share available to each nucleus. The poor distribution of PP spherulites was inherited from the distribution of crosslinked elastomer particles as nucleating sites.

References

1. Patel J, Maiti M, Naskar K, Bhowmick AK (2005) Novel styrenic thermoplastic elastomers from blends with special reference to compatibilization and dynamic vulcanization Rubber Chem Technol 78(5):893

2. KE Kear (2003) Developments in thermoplastic elastomers. Rapa Technology Limited Shrewsbury

3. Abdou-Sabet S, Puydak R, Rader C (1996) Dynamically vulcanized thermoplastic elastomers Rubber Chem Technol 69(3):476

4. Winters R, Lugtenburg J, Litvinov V, van Duin M, De Groot H (2001) Solid state 13 C NMR spectroscopy on EPDM/PP/oil based thermoplastic vulcanizates in the melt Polymer 42(24):9745

5. Tian M, Han J, Zou H, Tian H, Wu H, She Q, Chen W, Zhang L (2012) Dramatic influence of compatibility on crystallization behavior and morphology of polypropylene in NBR/PP thermoplastic vulcanizates J Polym Res 19(1):1

6. Howard MP, Milner ST (2013) Calculated interfacial free energies and heterogeneous nucleation of isotactic polypropylene Macromolecules 46(16):6600

7. Zhang X, Xie F, Pen Z, Zhang Y, Zhang Y, Zhou W (2002) Effect of nucleating agent on the structure and properties of polypropylene/poly (ethylene–octene) blends Eur Polym J 38(1):1

8. Papageorgiou GZ, Terzopoulou Z, Achilias DS, Bikiaris DN, Kapnisti M, Gournis D (2013) Biodegradable poly (ethylene

succinate) nanocomposites. Effect of filler type on thermal behaviour and crystallization kinetics Polymer 54(17):4604

9. Sattari M, Molazemhosseini A, Naimi-Jamal M, Khavandi A (2014) Nonisothermal crystallization behavior and mechanical properties of PEEK/SCF/nano-SiO$_2$ composites Mater Chem Phys 147(3):942

10. Avalos-Belmontes F, Ramos-deValle L, Ramírez-Vargas E, Sánchez-Valdes S, Méndez-Nonel J, Zitzumbo-Guzmán R (2012) Nucleating effect of carbon nanoparticles and their influence on the thermal and chemical stability of polypropylene J Nanomater 2012:104

11. Hoffman JD, Weeks JJ (1962) Melting process and the equilibrium melting temperature of polychlorotrifluoroethylene J Res Natl Bur Stand 66(1):13

12. L. Mandelkern. (1964) Crystallization of polymers. McGraw-Hill

13. J.D Hoffman, G.T Davis, J.I Lauritzen Jr. (1976) The rate of crystallization of linear polymers with chain folding, In Treatise in solid state chemistry, N.B Hannay, editor. Plenum Press

14. Šmit I, Denac M, Švab I, Radonjič G, Musil V, Jurkin T, Pustak A (2010) Structuring of polypropylene matrix in composites Polimeri 30(4):183

15. Ofora PU, Eboatu AN, Arinze RU, Nwokoye JN (2014) Effects of fillers of animal origin on the physico-mechanical properties of utility polymer IOSR J Appl Chem 7:19

16. Krikorian V, Pochan DJ (2004) Unusual crystallization behavior of organoclay reinforced poly (L-lactic acid) nanocomposites Macromolecules 37(17):6480

17. Uthaipan N, Jarnthong M, Peng Z, Junhasavasdikul B, Nakason C, Thitithammawong A (2015) Effects of cooling rates on crystallization behavior and melting characteristics of isotactic polypropylene as neat and in the TPVs EPDM/PP and EOC/PP Polym Test 44:101

18. Cyras VP, Rozsa C, Galego N, Vázquez A (2004) Kinetic expression for the isothermal crystallization of poly (3-hydroxybutyrate)–11% poly (3-hydroxyvalerate) J Appl Polym Sci 94(4):1657

19. De Santis F, Pantani R (2013) Nucleation density and growth rate of polypropylene measured by calorimetric experiments J Ther Anal Calorimetry 112(3):1481

20. Olley R, Bassett D (1982) An improved permanganic etchant for polyolefines Polymer 23(12):1707

21. Yadav Y, Jain P (1986) Melting behaviour of isotactic polypropylene isothermally crystallized from the melt Polymer 27(5):721

22. Zhao Y, Yuan G, Roche P, Leclerc M (1995) A calorimetric study of the phase transitions in poly (3-hexylthiophene) Polymer 36(11):2211

23. El-Shafee E, Saad GR, Fahmy SM (2001) Miscibility, crystallization and phase structure of poly (3-hydroxybutyrate)/cellulose acetate butyrate blends Eur Polym J 37(10):2091

24. Causin V, Yang BX, Marega C, Goh SH, Marigo A (2009) Nucleation, structure and lamellar morphology of isotactic polypropylene filled with polypropylene-grafted multiwalled carbon nanotubes Eur Polym J 45(8):2155

25. Papageorgiou GZ, Guigo N, Tsanaktsis V, Papageorgiou DG, Exarhopoulos S, Sbirrazzuoli N, Bikiaris DN (2015) On the bio-based furanic polyesters: Synthesis and thermal behavior study of poly (octylene furanoate) using fast and temperature modulated scanning calorimetry Eur Polym J 68:115

26. Abadchi MR, Jalali-Arani A (2015) Crystallization and melting behavior of polypropylene (PP) in (vulcanized nanoscale polybutadiene rubber powder/PP) polymer-nanocomposites Thermochim Acta 617:120

27. Clark EJ, Hoffman JD (1984) Regime III crystallization in polypropylene Macromolecules 17(4):878

28. Monasse B, Haudin JM (1985) Growth transition and morphology change in polypropylene Colloid Polym Sci 263(10):822

29. Grozdanov A, Bogoeva-Gaceva G, Avella M (2002) Quantitative evaluation of iPP nucleation in the presence of carbon fibres: induction time approach J Serb Chem Soc 67(12):843

30. Uthaipan N, Jarnthong M, Peng Z, Junhasavasdikul B, Nakason C, Thitithammawong A (2016) Micro-scale morphologies of EPDM/EOC/PP ternary blends: relating experiments to predictive theories of dispersion in melt mixing Mater Des 100:19

31. Young T (1805) An essay on the cohesion of fluids Phil Trans R Soc London 95:65

32. Dobreva A, Gutzow I (1993) Activity of substrates in the catalyzed nucleation of glass-forming melts II Exp Evid J Non-Cryst Solids 162(1):13

33. Dobreva A, Gutzow I (1993) Activity of substrates in the catalyzed nucleation of glass-forming melts I Theory J Non-Cryst Solids 162(1–2):1

34. Vassiliou AA, Papageorgiou GZ, Achilias DS, Bikiaris DN (2007) Non-Isothermal crystallisation kinetics of in situ prepared poly (ε-caprolactone)/surface-treated SiO2 nanocomposites Macromol Chem Phys 208(4):364

35. Hao W, Yang W, Cai H, Huang Y (2010) Non-isothermal crystallization kinetics of polypropylene/silicon nitride nanocomposites Polym Test 29(4):527

36. Assouline E, Lustiger A, Barber A, Cooper C, Klein E, Wachtel E, Wagner H (2003) Nucleation ability of multiwall carbon nanotubes in polypropylene composites J Polym Sci B Polym Phys 41(5):520

37. Alonso M, Velasco J (1997) Constrained crystallization and activity of filler in surface modified talc polypropylene composites Eur Polym J 33(3):255

38. Lim BA, McGuire KS, Lloyd DR (1993) Non-isothermal crystallization of isotactic polypropylene in dotriacontane. II: Effects of dilution, cooling rate, and nucleating agent addition on growth rate Polym Eng Sci 33:537

39. Xu JT, Zhao YQ, Wang Q, Fan ZQ (2005) Observation of regime III crystallization in polyethylene/montmorillonite nanocomposites Macromol Rapid Commn 26:620

40. Antoniadis G, Paraskevopoulos KM, Vassiliou AA, Papageorgiou GZ, Bikiaris D, Chrissafis K (2001) Nonisothermal melt-crystallization kinetics for in situ prepared poly (ethylene terephthalate)/monmorilonte (PET/OMMT) Thermochim Acta (1):521, 161

41. Zhou Z, Cui L, Zhang Y, Zhang Y, Yin N (2008) Isothermal crystallization kinetics of polypropylene/POSS composites J Polym Sci Part B Polym Phys 46(17):762

42. Papageorgiou GZ, Achilias DS, Bikiaris DN, Karayannidis GP (2005) Crystallization kinetics and nucleation activity of filler in polypropylene/surface-treated SiO$_2$ nanocomposites Thermochim Acta 427(1):117

43. Verma P, Choudhary V (2015) Polypropylene random copolymer/MWCNT nanocomposites: isothermal crystallization kinetics, structural, and morphological interpretations J Appl Polym Sci 132(13):1

44. Kocic N, Kretschmer K, Bastian M, Heidemeyer P (2012) The influence of talc as a nucleation agent on the nonisothermal crystallization and morphology of isotactic polypropylene: the application of the Lauritzen–Hoffmann, Avrami, and Ozawa theories J Appl Polym Sci 126(4):1207

45. Brown R, Eby R (1964) Effect of crystallization conditions and heat treatment on polyethylene: lamellar thickness, melting temperature, and density J Appl Phys 35(4):1156

46. Collette JW, Tullock CW, MacDonald RN, Buck WH, Su AC, Harrell JR, Mulhaupt R, Anderson BC (1989) Elastomeric polypropylenes from alumina-supported tetraalkyl Group IVB catalysts. 1. Synthesis and properties of high molecular weight stereoblock homopolymers Macromolecules 22(10):3851

47. Flores A, Aurrekoetxea J, Gensler R, Kausch H, Calleja FB (1998) Microhardness-structure correlation of iPP/EPR blends: Influence

of molecular weight and EPR particle content Colloid Polym Sci 276(9):786

48. Supaphol P, Spruiell JE (2002) Nonisothermal bulk crystallization of high-density polyethylene via a modified depolarized light microscopy technique: Further analysis J Appl Polym Sci 86(4):1009

49. Supaphol P, Spruiell JE, Lin JS (2000) Isothermal melt crystallization and melting behaviour of syndiotactic polypropylene Polym Int 49(11):1473

50. Baldenegro-Perez LA, Navarro-Rodriguez D, Medellin-Rodriguez FJ, Hsiao B, Avila-Orta CA, Sics I (2014) Molecular weight and crystallization temperature effects on poly (ethylene terephthalate) (PET) homopolymers, an isothermal crystallization analysis Polymer 6(2):583

51. Tian M, Li T, Zhang L, Tian H, Wu Y, Ning N (2014) Interfacial crystallization and its mechanism in in-situ dynamically vulcanized iPP/POE blends Polymer 55(13):3068

52. Gedde UW (1999) Microscopy of polymers. Springer, In Polymer physics,

53. Mansfield M, Boyd RH (1978) Molecular motions, the α relaxation, and chain transport in polyethylene crystals J Polym Sci Polym Phys Ed 16(7):1227

54. Warren BE (1941) X-Ray diffraction methods J Appl Phys 12(5):375

55. Ma LF, Wang WK, Bao RY, Yang W, Xie BH, Yang MB (2013) Toughening of polypropylene with β-nucleated thermoplastic vulcanizates based on polypropylene/ethylene–propylene–diene rubber blends Mater Des 51:536